# INFRARED-FREQUENCY COPLANAR STRIPLINES: DESIGN, FABRICATION, AND MEASUREMENTS

**Tasneem Mandviwala,[1,2] Brian Lail,[1] and Glenn Boreman[1,2]**
[1] Department of Electrical and Computer Engineering
University of Central Florida
4000 Central Florida Blvd.
Bldg #53, PO Box 162700
Orlando, FL 32816-2700
[2] College of Optics & Photonics/CREOL
University of Central Florida
Orlando, FL

*Received 30 March 2005*

**ABSTRACT:** *We investigate the feasibility of coplanar striplines (CPSs) in conjunction with infrared (IR) detectors. Because of unique attenuation and dispersion issues, the analytical formulas for transmission-line parameters valid below a few hundred GHz are not applicable at IR. Therefore, we perform numerical modeling to determine these parameters (at 28.3 THz). A comparison of the modeling and the measured response is presented.* © 2005 Wiley Periodicals, Inc. Microwave Opt Technol Lett 47: 17–20, 2005; Published online in Wiley InterScience (www.interscience.wiley.com). DOI 10.1002/mop.21068

**Key words:** *coplanar striplines; IR detectors; antenna response; infrared frequency; transmission line parameters*

## 1. INTRODUCTION

A variety of infrared spectroscopic and imaging applications require fast photodetectors. Since the response time of a photodetector is proportional to its volume, it seems reasonable to reduce the detector volume until the desired time constant is attained. However, as the sensor gets smaller it loses its ability to collect radiation, thus adversely affecting its responsivity. One way of maintaining a reasonable responsivity while obtaining a fast response is to integrate the sensor with an antenna. This integrated detector architecture separates the radiation collection function from the detection function. The antenna collects the radiation and supplies an electrical signal at its terminals. This electric signal is fed into, and processed by, the sensor. The sensor must be impedance-matched to the antenna in order to ensure maximum energy transfer. The design of infrared antennas requires us to take into account effects that can be neglected at microwave frequencies. Resonance features are altered because the propagation of the current waves of THz-frequency antennas is affected by the large

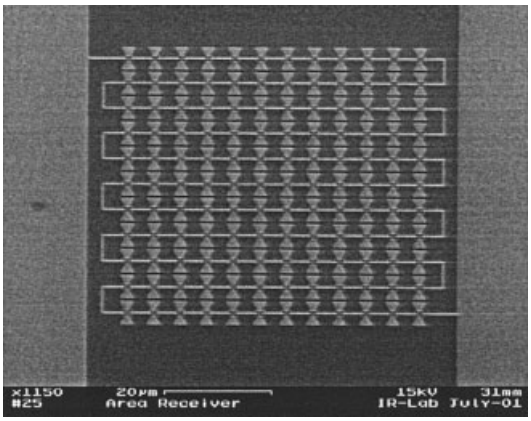


**Figure 1** Series connection of individual IR-antenna-coupled detectors

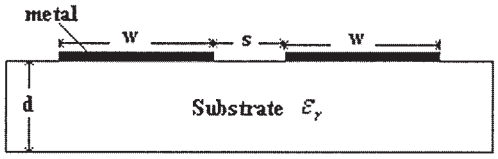


**Figure 2** Cross-sectional view of a coplanar stripline

high-frequency complex surface impedance of the metal. Fumeaux et al. [1] have studied niobium (Nb) microbolometers coupled to dipole antennas of several lengths in order to investigate the resonances of infrared dipole antennas on a SiO2-on-Si substrate.

One of the applications of using transmission lines in conjunction with IR detectors is in fabrication of phased-array antennas. Infrared focal-plane arrays that have been fabricated in the past (Fig. 1) consisted of antenna elements incoherently connected in series. With this interconnection, the current wave from individual sensors adds up, but phase information across the array is not preserved. Hence, this IR antenna would not work as a phased-array antenna. The advantages of phased-array antennas are that the reception beam narrows as the array becomes larger and the reception beam can be steered by controlling the phase difference between individual antennas.

This has motivated the study of interconnections suitable for IR-frequency current waves that will add each antenna's current along with preservation of phase information. The resulting aggregate current would then be sensed with a single sensor. The frequency range above a few hundreds of GHz well exceed the range of validity of the quasi-static approximations that are often made in modeling the propagation of electrical signals on transmission-line interconnects [2]. Also, the measurements of the transmission-line propagation properties have been applied to more fundamental studies such as the extraction of material parameters for high-temperature superconducting films in subterahertz frequency regions [3].

Figure 2 shows the configuration of a coplanar stripline (CPS) and the associated parameters: $w$ is the strip width, $s$ is the slot width, and $d$ is the thickness of the substrate having relative permittivity $\varepsilon_r$.

The propagation factor of a transmission line, in general, is given by

$$\gamma(f) = \alpha(f) + j\beta(f),$$

where $\alpha$ and $\beta$ are the attenuation and phase constants, respectively. The former mainly arises from the radiation, conductor, and dielectric losses, where the dielectric loss dominates when the substrate is highly conductive. The latter term, which determines the degree of dispersion a signal experiences, is affected primarily by the geometry of the transmission line, its dimensions, and the substrate permittivity.

Experiments have been conducted in the past to study the attenuation and dispersion characteristics of transmission lines below 1 THz. Mittleman et al. have studied the propagation of terahertz pulses (up to 1 THz) on metal wires and have found low loss and negligible dispersion [4]. Grischkowsky et al. have experimentally demonstrated that the radiative losses are dominant at frequencies over ~200 GHz for coplanar transmission-line dimensions of the order of few tens of microns [5]. Discrepancies between the radiative attenuation derived based on quasi-static approximation and that measured at frequencies ranging from 100 GHz to 1 THz is also found in the literature [2, 6]. In addition, the

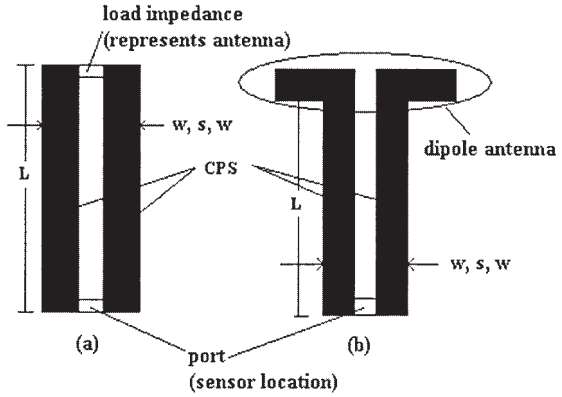


**Figure 3** (a) CPS model to estimate characteristic impedance and attenuation constant; (b) model for calculating current response

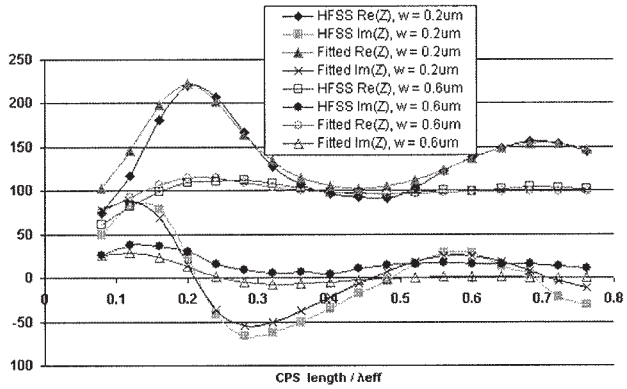


**Figure 4** Curve-fitting of HFSS data to Eq. (1) for $\omega = 0.2$ $\mu$m and 0.6 $\mu$m

attenuation characteristics highly depend on the type of substrate, for example, strong attenuation was observed for lossy semiconductor substrates [7] while virtually no attenuation and much lower dispersion was observed for CPS on low-permittivity substrates (that is, when there is less permittivity mismatch between the substrate and air) [8].

In order to study the characteristics and behavior of coplanar striplines at IR, we perform modeling, fabrication, and testing of a dipole resonating at 28.3 THz, connected to CPS of different lengths. We have done the numerical modeling of CPS using Ansoft HFSS, which is based on finite-element analysis. The numerical results of the port current as a function of CPS length are compared with the measured IR voltage response. This is the first LWIR transmission-line response measurement.

## 2. NUMERICAL CHARACTERIZATION OF CPS

Figure 3(a) shows the HFSS model of a given CPS structure. We model Au-CPS on 1.19-$\mu$m-thick SiO2 layer (quarter-wave thick in SiO2 at 10.6-$\mu$m wavelength) on top of 380-$\mu$m-thick Si wafer. One end of the CPS is connected to load impedance $Z_L$, which represents the antenna, while the other end is connected to the port. We estimate the CPS parameters in two steps as follows: (i) compute the input impedance at the port as a function of CPS length $L$, keeping the strip width $w$ and separation $s$ constant, and (ii) fit the impedance versus CPS length curve thus obtained to the impedance-transformation equation, given by

$$Z_{in} = Z_o\left(\frac{Z_L\cosh(\gamma.L) + Z_o\sinh(\gamma.L)}{Z_o\cosh(\gamma.L) + Z_L\sinh(\gamma.L)}\right), \quad (1)$$

where

$$\gamma = \alpha + j\beta,$$

$$\beta = \frac{2\pi}{\lambda_{eff}},$$

$$\lambda_{eff} = \frac{\lambda_o}{n_{eff}},$$

where $Z_o$ is the characteristic impedance of CPS, $Z_{in}$ is the input impedance at port, $\lambda_0$ is the freespace wavelength, and $\lambda_{eff}$ and $n_{eff}$ ($n_{eff} = 1.7$) are the effective wavelength and refractive index, respectively, in the substrate (200-nm SiO2 on Si). $Z_o$ and $\alpha$ are obtained by fitting the impedance-transformation equation to the data obtained from HFSS by simultaneously varying these two unknowns. Each unknown has a particular effect on the $Z_{in}$ versus CPS length curve; for example, the value of $Z_o$ defines the peak of the curve while $\alpha$ defines the damping. This procedure is repeated for different CPS widths $w$, and characteristic impedance and attenuation for each design is estimated. Figure 4 shows the curve fitting and extracted parameters for CPS widths of 0.2 $\mu$m and 0.6 $\mu$m, separation of 0.4 $\mu$m, and $Z_L = 50\Omega$. We find that as we increase the CPS width while keeping the separation constant, the characteristic impedance decreases and the attenuation constant increases, as shown in Figure 5.

Next, we replace the load impedance $Z_L$ by a dipole resonating at 28.3 THz ($\lambda_0 = 10.6$ $\mu$m) in our model in order to calculate the current at the port (response) as a function of CPS length $L$ [Fig. 3(b)]. The calculated normalized response is shown in Figure 8 below.

## 4. FABRICATION OF DIPOLE ANTENNA CONNECTED TO CPS

We fabricated a dipole antenna resonating at 28.3 THz, connected to CPSs of different lengths ranging from 0 to 5.75 $\mu$m in steps of 0.25 $\mu$m [Fig. 3(b) and Fig. 6]. All the devices in this study were patterned on 3-in., 380-$\mu$m-thick low-resistivity silicon substrates, with 1.19 $\mu$m of SiO2 for thermal and electrical isolation. The dipole arms are 0.6-$\mu$m wide and each arm length is 1.5 $\mu$m, with a separation of 400 nm between the arms. The width of the CPSs is 0.6 $\mu$m and the separation between them is 400 nm. A bolo-

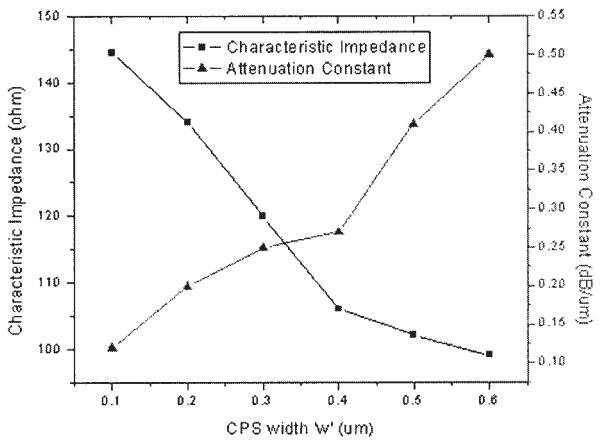


**Figure 5** $Z_o$ and $\alpha$ as a function of $\omega$ for $s = 0.4$ $\mu$m

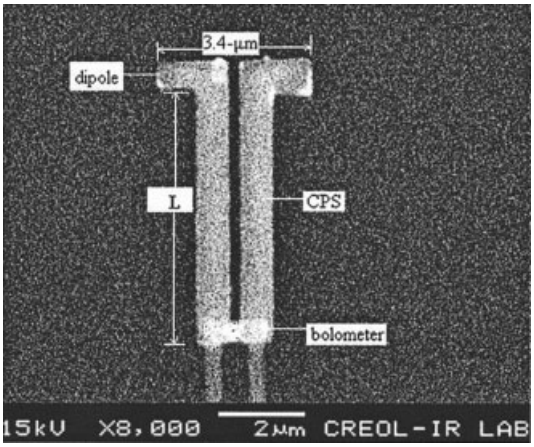


**Figure 6** Fabricated CPS-connected dipole

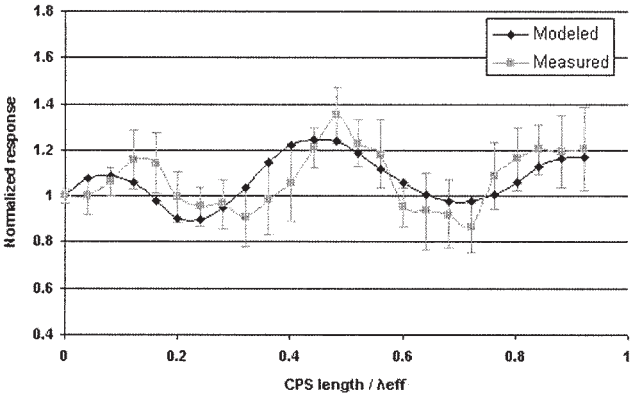


**Figure 8** Device response (measured: average and standard deviation for four devices at each point)

metric detector, 1.2 × 0.5 $\mu$m, was fabricated at the other end of the CPSs and 20-nm-wide and approximately 25-$\mu$m-long bias lines connect the CPSs to the bondpads for DC biasing of bolometer.

The substrates were spin-coated with a bilayer of copolymer (PMMA-MAA) and PMMA. A 350-nm layer of copolymer was obtained by spin-coating at 2000 rpm for 60 sec and baking on a hotplate at 180°C for 10 min. A second layer, 200-nm-thick PMMA, was spun onto the substrate at 3000 rpm for 1 min and baked afterwards for 10 min on a 180°C hotplate.

The antenna, bolometer, bond-pads, and bias lines were patterned using a Leica EBPG5000 electron-beam lithography system. The antennas, bias lines, and bondpads were written at a dose of 600 $\mu$C/cm$^2$ and with a beam current of 15 nA. The bolometers were written with an e-beam current of 5 nA at a dose of 700 $\mu$C/cm$^2$. After exposure, the devices were developed for 1 min in a 3:1 solution of IPA:MIBK, rinsed with IPA, and blow-dried with a nitrogen gun.

The antennas were made out of 100 nm of e-beam-evaporated gold (Au) over a 7-nm adhesion-layer of chromium (Cr) and lift-off was done using methylene chloride. The bolometers were made of 120 nm of RF-sputtered nickel (Ni), and the lift-off process was done using methylene chloride also.

## 5. EXPERIMENTAL METHOD AND RESULTS

We measured the voltage response of these devices (that is, the voltage at the bolometer versus CPS length). Other modeled parameters such as characteristic impedance and attenuation constant cannot be measured directly in the laboratory. Based on the information from the measured response, we can relate the characteristic impedance and input impedance, as well as the response plots obtained from modeling, because the voltage response depends on the impedance transformation at the sensor, which in turn is related to the characteristic impedance of CPS. Thus, our response measurement can be related to the modeled characteristic impedance and attenuation constant and their validity can be confirmed.

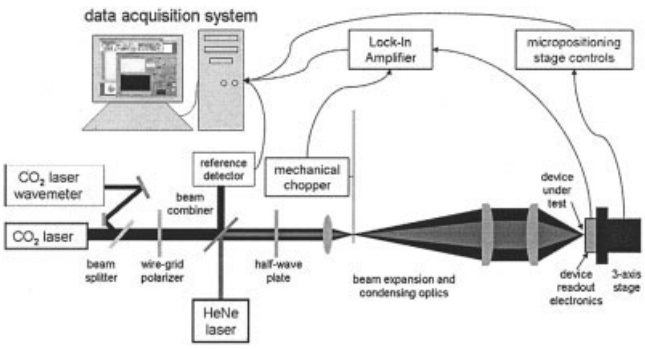


**Figure 7** Test setup for response measurement

The device measurement was carried out using the test setup shown in Figure 7. The $CO_2$ laser beam at 10.6-$\mu$m emission was focused by an F/8 optical train. The polarization was linear and was rotated by means of a half-wave plate (HWP). The bolometer under test was biased at 100 mV and placed at the focus of the laser beam. The position of the device was adjusted for best response using motorized stages with submicron accuracy. The laser beam was modulated with a chopper at a frequency of 2.5 kHz and the modulated signal produced by the bolometer was read with a lock-in amplifier after a 1000× preamplification. For each device, the response $V_{\|}$ to radiation polarized along the dipole arm was measured at normal incidence.

Figure 8 shows a comparison between the normalized modeled port current and the measured bolometer voltage response as a function of CPS length. Both these quantities are comparable, since the current couples thermally in the bolometer and the changes in the resistance of the sensor material produces measurable changes in an external bias voltage. The modeled and measured quantities are in good agreement.

## 6. CONCLUSION

The CPS interconnection for an antenna at IR frequencies has been studied. The characteristic impedance and attenuation constant were computed for different CPS designs using HFSS. We found an increase in attenuation and a decrease in characteristic impedance as we increase the CPS width. The sensor response (current at the port) was computed as a function of CPS length in order to relate it to the transmission-line parameters. The modeled device response was compared to the measured response with good agreement. Figure 8 depicts the transmission-line behavior of CPS at LWIR frequencies in the vicinity of 30 THz.

## REFERENCES

1. C. Fumeaux, M. Gritz, I. Codreanu, W. Schaich, F.J. González, and G. Boreman, Measurement of the resonant lengths of infrared dipole antennas, Infrared Phys Tech 41 (2000), 271–281.
2. M.Y. Frankel, S. Gupta, J.A. Valdmanis, and G.A. Mourou, Terahertz, attenuation, and dispersion characteristics of coplanar transmission lines, IEEE Trans MTT 39 (1991), 910–916.
3. D.R. Dykaar, et al., High-frequency characterization of thin-film Y-

Ba-Cu oxide superconducting transmission lines, Appl Phys Lett 52 (1988), 1444–1446.
4. K. Wang and D. Mittleman, Metal wire waveguides for broadband terahertz pulses, 17th Ann IEEE LEOS Mtg, 2004.
5. D. Grischkowsky, I.N. Duling III, J.C. Chen, and C.C. Chi, Electromagnetic shock waves from transmission lines, Phys Rev Lett 59 (1987), 1663–1666.
6. D.B. Rutledge, D.P. Neikirk, and D.P. Kasilingham, K.J. Button (Ed.) Infrared and millimeter waves 10 (II) Academic, New York, 1983.
7. J.H. Son, H.H. Wang, J.F. Whitaker, and G.A. Mourou, Picosecond pulse propagation on coplanar striplines fabricated on lossy semiconductor substrates: Modeling and experiments, IEEE Trans MTT 41 (1993), 1574–1580.
8. H.J. Cheng, J.F. Whitaker, T.M. Weller, and L.P.B. Katehi, Terahertz-bandwidth characteristics of coplanar transmission lines on low-permittivity substrates, IEEE Trans MTT 42 (1994), 2399–2406.



# A NOVEL GENETIC-ALGORITHM-BASED ARTIFICIAL MAGNETIC CONDUCTOR STRUCTURE

**Gao Qiang, Dun-Bao Yan, Yun-Qi Fu, and Nai-Chang Yuan**
Microwave Center
School of Electronic Science and Engineering
National University of Defense Technology
Changsha, HuNan Province 410073, P. R. China

*Received 29 March 2005*

**ABSTRACT:** *In this paper, a novel genetic algorithm (GA)-based AMC structure, which is made up of a high-impedance frequency-selective surface, is introduced. The aperture-coupled microstrip antenna using this structure has 10-dB less back radiation and 3–4-dB more gain than a conventional one. This structure has important reference value for antenna manufacturing. A practical antenna is fabricated, and the measured results basically agree well with the simulated ones.* © 2005 Wiley Periodicals, Inc. Microwave Opt Technol Lett 47: 20–22, 2005; Published online in Wiley InterScience (www.interscience.wiley.com). DOI 10.1002/mop.21069

**Key words:** *genetic algorithm; artificial magnetic conductor (AMC); high-impedance frequency-selective surface (HZ-FSS); aperture-coupled microstrip antenna*

## 1. INTRODUCTION

It is well known that a hypothetical perfectly magnetic conductor may be very useful in a large variety of microwave applications; for instance, a magnetic ground plane can improve the performance of dipole antennas by creating their equiverse image currents. In recent years, photonic bandgap structures have been widely investigated for their behavior as artificial magnetic conductors (AMCs) at the corresponding stopband frequency [1]. The specific AMC designs reported in [2] utilized a high-impedance frequency-selective surface (HZ-FSS) geometry consisting of a single substrate layer between the FSS screen and the PEC ground plane. This configuration is desirable for its low manufacturing cost and easy integration in microwave devices.

Genetic algorithms (GAs) are a special class of global optimization schemes that consistently exhibit robust performance and therefore enjoy a wide range of applications in the design of electromagnetic systems. In this paper, we apply a specific GA formulation to the problem of designing AMCs in conjunction with an electromagnetic solver based on the method of moments (MoM). An example shows that the use of such a surface, in lieu of the conventional PEC ground plane, leads to an improvement in the directivities of an aperture-coupled microstrip antenna.

## 2. FORMULATION

Firstly, we consider the formulation of scattering from an FSS in the spectral domain. An MoM-based computer code has been employed to perform the electromagnetic simulations of the FSS. The numerical analysis follows the well-established procedure of solving the electric-field integral equation (EFIE) for the current distribution on perfectly conducting patches, derived by enforcing Floquet's periodicity condition in an elementary cell [3]. Consider a screen lying in the $x$–$y$ plane, with cell periodicities $d_x$ and $d_y$ along the $x$ and $y$ directions, respectively. Then we can cast the EFIE in the following form:

$$\begin{bmatrix} -E_x^{inc}(x,y) \\ -E_y^{inc}(x,y) \end{bmatrix} = \frac{1}{j\omega\varepsilon_0} \sum_{m,n=-\infty}^{m,n=+\infty} \begin{bmatrix} k_0^2 - \alpha_m^2 & -\alpha_m\beta_n \\ -\alpha_m\beta_n & k_0^2 - \beta_n^2 \end{bmatrix} \cdot \tilde{\bar{G}}(\alpha_m, \beta_n) \times \begin{bmatrix} \tilde{J}_x(\alpha_m, \beta_n) \\ \tilde{J}_y(\alpha_m, \beta_n) \end{bmatrix} e^{j(\alpha_m x + \beta_n y)}. \quad (1)$$

Eq. 1 must be solved for the unknown current distributions $J_x$and $J_y$, which are expressed in terms of a set of subdomain basis functions known as 'rooftops' that are particularly suited for handling arbitrarily shaped patches [3]. Next, a matrix equation is derived by applying the Galerkin procedure and is solved for the current distribution. The FSS response is then computed from the knowledge of this distribution.

The AMC in this paper consists of a single substrate layer between the FSS screen and the PEC ground plane. To conveniently analyze it using a GA, we resort to using the scattering-matrix technique [4]. The generalized scattering matrices of the individual FSS screens can be derived using the MoM. These matrices can be subsequently used to generate a composite scattering matrix for the entire system using the following relationships:

$$\begin{aligned} S_{11}^C &= S_{11}^{(1)} + S_{12}^{(1)} R S_{11}^{(2)} S_{21}^{(1)}, \\ S_{12}^C &= S_{12}^{(1)} R S_{12}^{(2)}, \\ S_{21}^C &= S_{21}^{(2)} T S_{21}^{(1)}, \\ S_{22}^C &= S_{22}^{(2)} + S_{21}^{(2)} T S_{22}^{(1)} S_{12}^{(2)}, \end{aligned} \quad (2)$$

where $R = [I - S_{11}^{(2)} S_{22}^{(1)}]^{-1}$, $T = [I - S_{22}^{(1)} S_{11}^{(2)}]^{-1}$, and the superscripts are associated with the two subcomposites. For PEC, $[S_{11}^{(2)}] = [S_{22}^{(2)}] = -I$, $[S_{12}^{(2)}] = [S_{21}^{(2)}] = [0]$. GA [5] is employed to synthesize an optimal, PEC-backed, FSS element whose reflection coefficient is close to unity in magnitude and 0° in phase. The FSS cells, which will be printed on the substrate with $\varepsilon_r = 10.2$ and $h = 4$ mm, have the fixed dimensions: $d_x = d_y = 4.8$ mm.

The only optimization parameter is a discretised mask of the printed element in the basic periodic cell, which is subdivided into elementary pixels coded as 1s or 0s, depending on whether or not they are covered by a printed metal. The fitness function has been chosen in the following form:

$$F = \alpha \cdot F^{\text{freq}} + (1 - \alpha) \cdot F^{\text{inc}}, \quad (3)$$

where $0 \le \alpha \le 1$,